Front. Earth Sci. 2016, 10(1): 29–37
DOI 10.1007/s11707-015-0502-y

RESEARCH ARTICLE

Experimental study of the effect of shallow groundwater table on soil thermal properties

Jianmei JIANG[1], Lin ZHAO (✉)[1,2], Yijian ZENG[3], Zhe ZHAI[2]

1 School of Chemical Engineering, Tianjin University, Tianjin 300072, China
2 School of Environmental Science and Engineering, Tianjin University, Tianjin 300072, China
3 Water Resources Department, ITC Faculty, University of Twente, Enschede 7514 AE, Netherlands

Abstract In plains areas with semi-arid climates, shallow groundwater is one of the important factors affecting soil thermal properties. In this study, soil temperature and water content were measured when groundwater tables reached 10 cm, 30 cm, and 60 cm depths (Experiment I, II, and III) by using sensors embedded at depths of 5 cm, 10 cm, 20 cm, and 30 cm for 5 days. Soil thermal properties were analyzed based on the experimental data using the simplified de Vries model. Results show that soil water content and temperature have fluctuations that coincide with the 24 h diurnal cycle, and the amplitude of these fluctuations decreased with the increase in groundwater table depth. The amplitude of soil water content at 5 cm depth decreased from 0.025 $m^3 \cdot m^{-3}$ in Experiment II to 0.01 $m^3 \cdot m^{-3}$ in Experiment III. Moreover, it should be noted that the soil temperature in Experiment III gradually went up with the lowest value increasing from 26.0°C to 28.8°C. By contrast, the trends were not evident in Experiments I and II. Results indicate that shallow groundwater has a "cooling" effect on soil in the capillary zone. In addition, calculated values of thermal conductivity and heat capacity declined with the increasing depth of the groundwater table, which is consistent with experimental results. The thermal conductivity was stable at a value of 2.3 $W \cdot cm^{-1} \cdot K^{-1}$ in Experiment I. The average values of thermal conductivity at different soil depths in Experiment II were 1.82 $W \cdot cm^{-1} \cdot K^{-1}$, 2.15 $W \cdot cm^{-1} \cdot K^{-1}$, and 2.21 $W \cdot cm^{-1} \cdot K^{-1}$, which were always higher than that in Experiment III.

Keywords soil temperature, thermal property, groundwater table depth, evaporation

Received May 19, 2014; accepted October 15, 2014

E-mail: zhaolin@tju.edu.cn

1 Introduction

Knowledge of soil thermal properties is necessary for numerous engineering, environmental, and agronomical applications. Effective thermal conductivity, λ ($W \cdot m^{-1} \cdot K^{-1}$), has garnered much interest because it significantly affects the surface energy partitioning, temperature distribution, and moisture flow within soil and near-ground atmosphere systems (Karl, 1986; Chung and Horton, 1987; Heilman et al., 1996; Saito and Šimunek, 2009; Wang et al., 2010). Soil thermal conductivity is obtained by either laboratory or field methods (Barry-Macaulay et al., 2013). Experimental methods are commonly used instead of field methods because they are relatively inexpensive, quick, and allow for greater control over the boundary conditions. Laboratory approaches can be divided into steady state and transient state methods, in which the latter method is more suitable because of its relative simplicity and short measurement time. Transient methods such as the use of thermal conductivity probes are widely applied in calculating thermal conductivity of materials (Bristow et al., 2001; Waite et al., 2006; Daw et al., 2012; Yang et al., 2013). Researchers monitored the dissipation of heat to calculate the thermal conductivity by using the needle probe method, which is based on the infinite line heat source theory. Lu et al. (2013) estimated soil thermal properties from late-time data of the temperature change-by-time curve to reduce the heat pulse (HP) probe errors. However, thermal needle probes cannot accurately measure the changeable thermal conductivity of soil under non-isothermal evaporation conditions, which require a quantitative understanding of the coupled dependence on texture, temperature, and water content. A new system consisting of soil temperature sensors and soil moisture sensors embedded in the soil at a specific depth should be proposed to measure soil thermal conductivity. Soil temperature and

moisture sensors are usually applied to estimate the coupled water, vapor, and heat transport (Saito et al., 2006; Bittelli et al., 2008; Zeng et al., 2009, 2011a, b; Li et al., 2010), while they are also shown to estimate the soil thermal property very well (Kang et al., 2014).

By considering the solid uniform ellipsoidal particles within a fluid, soil thermal properties were estimated using the de Vries model with the assumption that soil is composed of two phases (de Vries, 1958, 1963). Cass et al. (1984) measured apparent soil thermal conductivity under various air pressures and developed a method to separate the contributions of conduction and latent heat transfer of vapor to the overall soil heat flow. Lu et al. (2011) treated conduction heat transfer as the apparent soil thermal conductivity associated with infinite atmospheric pressure. Nakhaei and Šimunek (2014) estimated thermal conductivity parameters from cumulative infiltration and temperature measurements by inversely solving a two-dimensional water flow and heat transport problem.

Soil thermal properties are influenced by a wide variety of parameters, including mineral composition, particle shape and size distribution, temperature, dry density, porosity, and water content (Usowicz et al., 2013). For the same soil texture, temperature and water content may be the main factors for thermal properties, both of which are not only influenced by climate or infiltration but also greatly affected by shallow groundwater through capillary action. As in many cases, a shallow groundwater table is critical in the agriculture over large-scale irrigation systems in various countries, including the United States, Mexico, China, India, Pakistan, Australia, etc (Umali, 1993; Rahman, 2008; Shi et al., 2010). Carrera-Hernández et al. (2012) estimated groundwater recharge with a coupled unsaturated soil water flow model, studied the effect of both discretization and boundary conditions on simulation time, and estimated fluxes at the water table. However, the exact effect of shallow groundwater on soil thermal properties is not well understood.

The primary objective of this paper is to present the direct effects of shallow groundwater on soil water content and temperature under non-isothermal evaporation conditions. The secondary objective is to estimate thermal properties by using the simplified de Vries model based on a temperature and soil moisture sensor technique, and to discuss the indirect influence of shallow groundwater on thermal properties.

2 Materials and methods

2.1 Experiments

Three experiments (I, II, III) with different groundwater table depths (i.e., 10 cm, 30 cm, and 60 cm) were conducted under non-isothermal evaporative demand, which was forced by two infrared tubes arranged in parallel on the insulation board, simulating the effect of the sun. The evaporation simulator was placed 80 cm above the soil surface. The heating power was 300 W. Irradiation time was from 8:30 to 17:30, similar to summer radiation at mid-latitudes.

The test apparatus was a 2 cm thick piece of Plexiglass 150 cm (length) × 50 cm (width) ×100 cm (height). The box was comprised of three parts: two side water boxes, each measuring 25 cm × 50 cm ×100 cm, used as inlets and outlets to adjust groundwater tables; and a middle box with dimensions of 100 cm × 50 cm × 100 cm used to fill soil samples (Fig. 1). The three parts were separated by Plexiglass with apertures to allow free water movement. Three experiments were conducted by using the same apparatus.

The soil samples were collected in the saline wasteland of China–Singapore eco-city, Tianjin, China. The samples were air-dried, ground, and sieved through a 10 mm sieve.

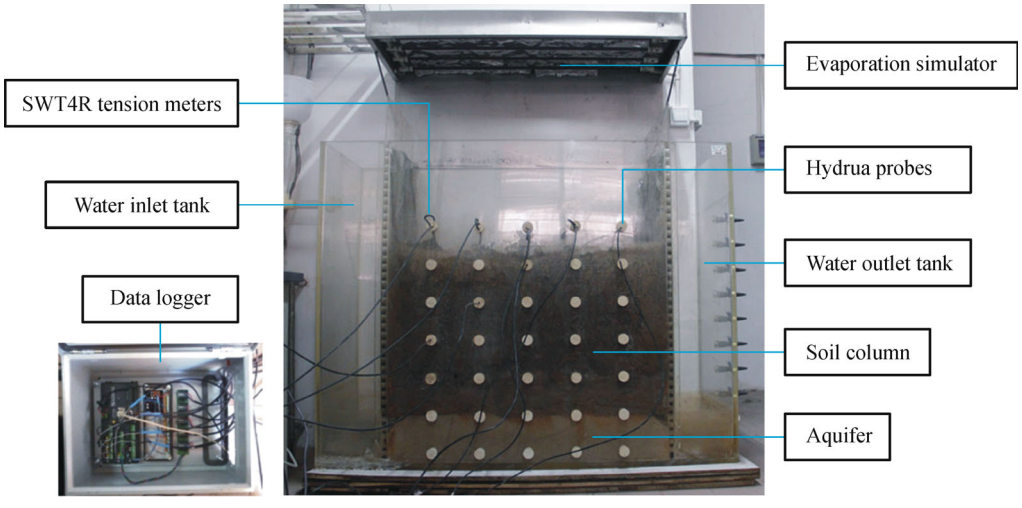

Fig. 1 Experimental setup for Experiment III (60 cm height of soil column).

Before packing the soil to thicknesses of 10 cm, 30 cm, and 60 cm, fine sand layers with different thickness were packed into the bottom of the soil columns to act as groundwater aquifers for the three experiments. Mesh was placed on the sand-soil layer boundary to avoid flow erosion. The samples were mixed thoroughly to minimize differences between different set-ups and packed into the box in 10 cm layers to achieve a natural bulk density of approximately 1.53 $g \cdot cm^{-3}$. Each soil layer was lightly raked prior to packing the next layer to minimize the discontinuity between layers. Finally the inlet and outlet water valves were opened to maintain a constant groundwater level. The capillary rise height was controlled at 23.5 cm before assessing soil temperature changes.

To monitor soil temperature and water content, Hydra probes with a length of 12.4 cm (Steven, USA) were inserted vertically into soil samples at depths of 5 cm, 10 cm, 20 cm, and 30 cm. Hydra probes have reported accuracies of ±0.6°C for temperature and ±3% for volume water content. Soil water potential was measured by SWT4R tension meters (Delta-T, England) that were obliquely embedded at the same depth as the Hydra probes. The tension meters have an accuracy of ±0.5 kPa. All temperature, water content, and water potential data were collected and recorded every 10 min by a data logger (CR1000, Campell, USA) and stored on a disk. Relative humidity (*RH*) and air temperature (*T*) above the soil surface were hourly measured by a psychrometer. The duration of each experiment was 5 days. Soil texture was characterized as silt loam on the basis of grain size distribution analysis. The van Genuchten analytical model (van Genuchten, 1980) was fitted to the retention data by using RETC code, leading to hydraulic parameters as in Table 1.

2.2 Model description

Total volumetric heat capacity of moist soil (C_p [$J \cdot m^{-3} \cdot K^{-1}$]) was defined as follows:

$$C_p = C_n + C_W + C_V, \tag{1}$$

where C_n, C_W, and C_V are the volumetric heat capacities ($J \cdot m^{-3} \cdot K^{-1}$) of solid, liquid water, and water vapor phases, respectively. The expression for the volumetric heat capacity of moist porous media was introduced as:

$$C_p = C_n + C_{P'} \rho_r \theta_a + C_L \rho_w \theta, \tag{2}$$

where $C_{p'}$ is the specific heat of water vapor at constant pressure ($J \cdot kg^{-1} \cdot K^{-1}$), ρ_r is the water vapor density ($kg \cdot m^{-3}$), θ_a is the volumetric air content ($m^3 \cdot m^{-3}$), C_L is the specific heat of liquid water ($J \cdot kg^{-1} \cdot K^{-1}$), ρ_w is the pure water density ($kg \cdot m^{-3}$), and θ is the volumetric water content in the liquid phase ($m^3 \cdot m^{-3}$).

The apparent thermal conductivity $\lambda(\theta)$ was expressed as follows (Lu et al., 2011):

$$\lambda(\theta) = \lambda_c + \lambda_v = \lambda_c + La a \eta D H_r \frac{d\rho^*}{dT}, \tag{3}$$

where $\lambda(\theta)$ is the apparent thermal conductivity of soil ($W \cdot m^{-1} \cdot K^{-1}$), λ_c is the thermal conductivity from conduction alone ($W \cdot m^{-1} \cdot K^{-1}$), λ_v is the thermal conductivity caused by latent heat transfer of vapor ($W \cdot m^{-1} \cdot K^{-1}$), L is the latent heat of vaporization ($J \cdot kg^{-1}$), a is the air-filled porosity ($m^{-3} \cdot m^{-3}$), α is the tortuosity factor (unitless), η is the mechanistic enhancement factor (unitless), D is the diffusion coefficient of water vapor in air ($m^2 \cdot s^{-1}$), H_r is the relative humidity, and ρ^* is the saturated vapor density ($kg \cdot m^{-3}$) . The λ_c accounts for the porous medium, and can be described with a simple equation given by Chung and Horton (1987):

$$\lambda_c = b_1 + b_2 \theta + b_3 \theta^{0.5}, \tag{4}$$

where b_1, b_2, and b_3 are empirical regression parameters ($W \cdot m^{-1} \cdot K^{-1}$), and θ is the volumetric water content ($m^3 \cdot m^{-3}$), Chung and Horton (1987) also provided average values for the b coefficients for three textural classes (i.e., clay, loam, and sand), which are implemented in the Hydrus-1D program (Šimunek et al., 1998; Saito and Šimunek, 2009; Deb et al., 2011).

The latent heat of vaporization of water, L, is described as follows (Novak, 2010):

$$L = 2.5 \times 10^6 - 2400(T - 273.15), \tag{5}$$

η was introduced by Philip and de Vries (1957) to account for the effect that the observed vapor flux density in response to a temperature gradient was significantly larger than what was predicted. Cass et al. (1984) developed an empirical model to estimate η from soil water content and porosity:

$$\eta = 9.5 + 3\frac{\theta}{\theta_s} - 8.5\exp\left\{-\left[\left(1 + \frac{2.6}{\sqrt{f_c}}\right)\frac{\theta}{\theta_s}\right]^4\right\}, \tag{6}$$

where f_c is the mass fraction of clay in the soil (unitless), θ is the volumetric water content ($m^3 \cdot m^{-3}$), and θ_s is the saturated volumetric water content ($m^3 \cdot m^{-3}$).

Table 1 Texture and hydraulic properties of soil samples in analysis

Particle-size distribution/%			ρ/($g \cdot cm^{-1}$)	θ_r/($cm^3 \cdot cm^{-3}$)	θ_s /($cm^3 \cdot cm^{-3}$)	α/(cm^{-1})	n
Sand	Silt	Clay	1.53	0.14	0.42	0.07	1.54
9	67	24					

Note: ρ is the soil bulk density, θ_r is the residual water content, θ_s is the saturated water content, α is related to the inverse of the air-entry pressure, and n is a measure of the pore-size distribution affecting the slope of the retention function (unitless).

The diffusivity of water vapor in air D ($m^2 \cdot s^{-1}$) at temperature T (K) is expressed as:

$$D = 2.12 \times 10^{-5} \left(\frac{T}{273.15} \right)^2, \quad (7)$$

where the relative humidity, H_r, can be calculated from the pressure head, h (m), using a thermodynamic relationship between liquid water and water vapor in soil pores (Philip and de Vries, 1957):

$$H_r = \exp\left(\frac{hMg}{RT} \right), \quad (8)$$

where M is the molecular weight of water (0.018015 $kg \cdot mol^{-1}$), g is the gravitational acceleration (9.81 $m \cdot s^{-1}$), and R is the universal gas constant (8.314 $J \cdot mol^{-1} \cdot K^{-1}$).

The derivative of ρ^* in Eq. (3) is defined as (Novak, 2010):

$$\frac{d\rho^*}{dT} = \frac{\rho^*}{T} \left[\frac{4098.17T}{(T-35.85)^2} - 1 \right]. \quad (9)$$

The saturated vapor density ρ^* is expressed by the empirical curve:

$$\rho^* = \frac{1.323}{T} \exp\left(\frac{17.27T - 4717.3}{T - 35.85} \right). \quad (10)$$

On the basis of the transient data measured for volumetric water content and soil temperature at different depths, heat capacity and thermal conductivity can be calculated from the above equations with empirical parameters.

3 Results and discussion

3.1 Capillary water rise measurements

The rise of capillary water should be recorded to determine the relative positions of monitoring depths and saturated soil zones before assessing soil temperature changes. The soil column height was 30 cm, which is the same as that in Experiment II. The result is also applicable to Experiments I and III because of the same soil texture and compactions.

Figure 2 shows the overall "fast then slow" trend of capillary water rise, with the final rise height of 23.5 cm in the static soil column after 8 days. The groundwater recharge rate decreased from 3.1 $cm \cdot d^{-1}$ to 0.9 $cm \cdot d^{-1}$, but not to zero. This interesting phenomenon is caused by soil water vapor conversion, which was recharged by groundwater under minimal evaporation in the laboratory. The result agrees with other research of Rose et al. (2005). They denoted that the contribution of the groundwater remained constant at 0.2 $cm \cdot d^{-1}$, which is the same as the evaporation rate at the soil surface above the 30 cm groundwater table. Thus, the initial evaporation from the soil surface reached steady state and equaled the shallow groundwater recharge.

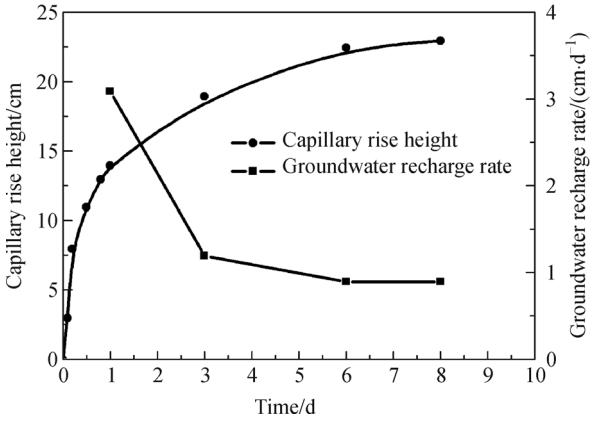

Fig. 2 Capillary water rise height and groundwater recharge rate variation in a static soil column with the height of 30 cm.

Results indicate that in Experiment I, the soil column was filled with capillary water; in Experiment II, the soil column was characteristic of saturated–unsaturated soil type (the upper observed layer 5 cm depth was in the unsaturated zone, whereas the rest was in the capillary zone); in Experiment III, all four observation layers (5 cm, 10 cm, 20 cm, and 30 cm depths) belonged to the unsaturated zones. Soil columns in three experiments, especially saturated and saturated–unsaturated types, were seldom studied in the past because researchers mostly focused on arid areas with groundwater located far below the soil surface (Kane et al., 2001; Grifoll et al., 2005; Saito and Šimunek, 2009; Zeng et al., 2009; Fan et al., 2011; Kanzari et al., 2012).

3.2 Soil water content

Figure 3 shows the moisture content observed at the 5 cm depth in the three experiments decreased with an increase in groundwater table depth. The moisture content fluctuated around 0.41 $m^3 \cdot m^{-3}$ when the groundwater table was at the 10 cm depth. This finding may be caused by near saturation of the soil with capillary water. Moisture content evidently correlates well with the 24 hour diurnal-cycle fluctuations for the unsaturated soil layer above 30 cm and 60 cm water table depths. The amplitude was less when groundwater depth was deeper. Therefore, the conversion of liquid and vapor was greater when the moisture content in the upper soil layer was larger. The average moisture content was 0.32 $m^3 \cdot m^{-3}$ with an amplitude of 0.025 $m^3 \cdot m^{-3}$ when the water table depth was 30 cm, while it was 0.24 $m^3 \cdot m^{-3}$ with amplitude of 0.01 $m^3 \cdot m^{-3}$ when the water table depth reached 60 cm.

Figure 4 shows the variation of water content in the soil profile above the 60 cm groundwater table. Results show that moisture content changed dramatically in the upper

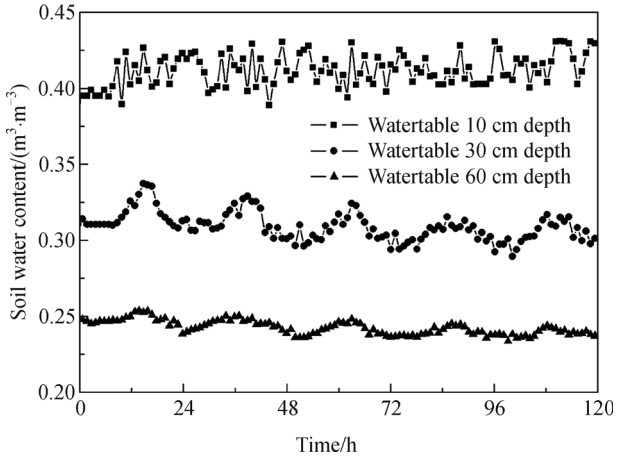

Fig. 3 Soil water content changes at 5 cm depth of soil profiles above 10 cm, 30 cm, and 60 cm groundwater tables.

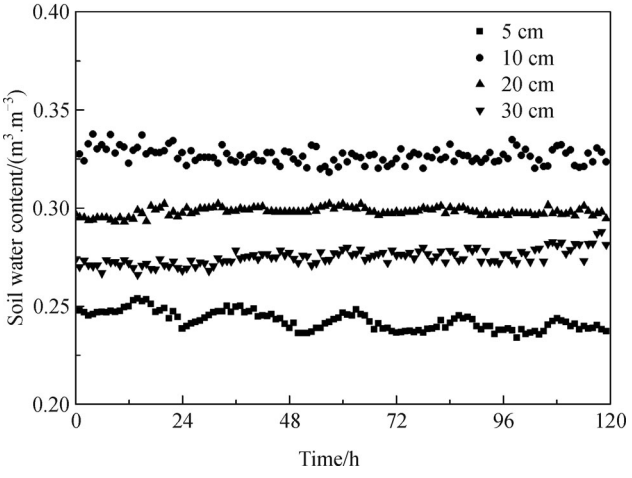

Fig. 4 Water content changes of soil profile above 60 cm groundwater table.

unsaturated soil layer (5 cm depth), but no change was evident in the deeper layers. The average soil moisture content was higher at the 10 cm depth than at other depths. This phenomenon is similar to the research reported by Kanzari et al. (2012). They found that higher water content occurred at a deeper depth of 2 m, which is influenced by the top soil material, with sandy (0 m to 0.6 m) to clay (0.6 m to 2 m) to sandy–silty (>2 m) texture. However, for homogeneous soil, soil water content increases with the increasing soil depth in the top layer (Rose, 1968; Grifoll et al., 2005). Results of the present study may be explained by nonuniform compaction of the soil layers across the entire profile. A measurement uncertainty of $\pm 3\%$ for Hydro probes most probably results in such phenomenon because water content does not vary much between soil layers.

3.3 Soil temperature profiles

Figure 5 shows that the soil temperature changes above the three different groundwater table depths. The soil temperature profiles are concurrent with the 24 h diurnal-cycle fluctuations. The specific results are as follows:

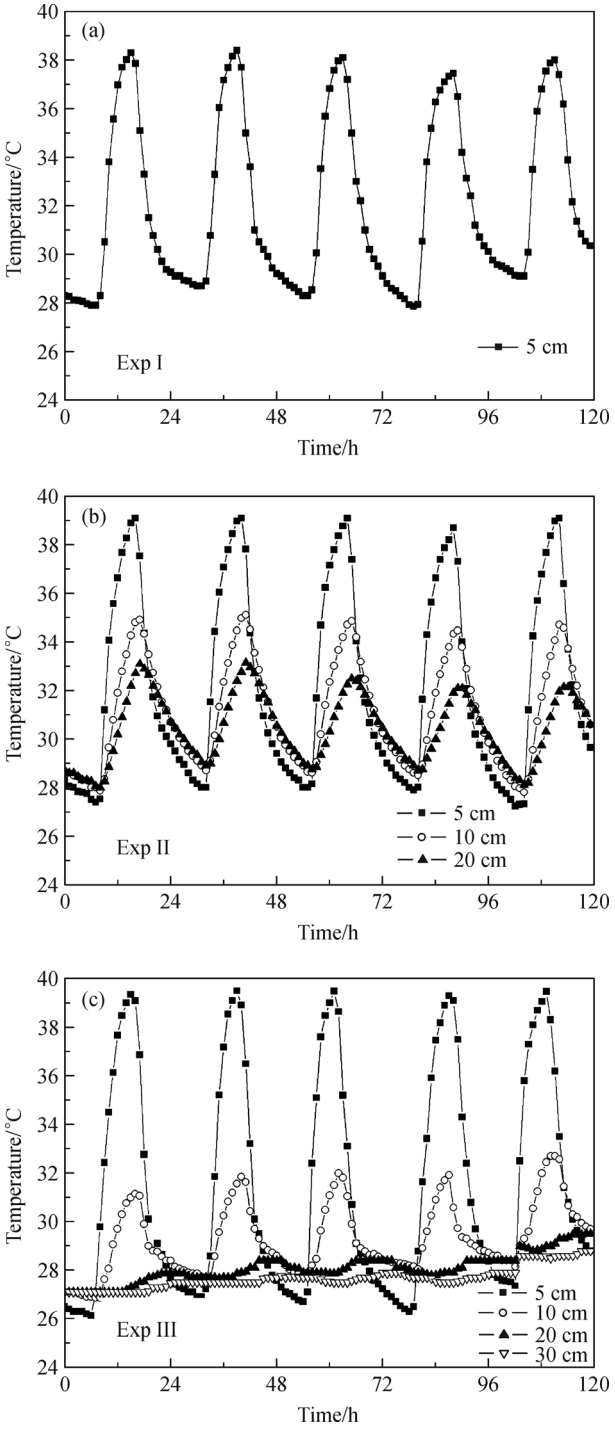

Fig. 5 Soil temperature at different depths above groundwater tables (a) 10 cm, (b) 30 cm, and (c) 60 cm deep.

In Experiment I (10 cm groundwater table depth), the soil temperature at 5 cm depth slowly decreased from 28.3°C at 0:00 to 27.9°C at 7:00. The temperature sharply increased to 38.4°C at 15:00 with a rate of 1.3°C·h^{-1}. Afterward, the temperature dropped until 23:00. At 19:00, soil temperature started to fall gradually after experiencing a rapid decrease. The trend of temperature variation is caused by the small temperature difference between the air and soil interior, which is similar to the field observations by other researchers (Bittelli et al., 2008; Zeng, 2011).

When the groundwater table depth was increased to 30 cm (Experiment II), the amplitudes of the fluctuating daily temperatures at the 5 cm, 10 cm, and 20 cm soil profile depths were about 10°C, 6°C, and 4°C, respectively, which were caused by soil moisture content at different depths. Lower soil moisture content and lower heat capacity lead to larger fluctuations in diurnal soil temperatures.

For the 60 cm groundwater table depth (Experiment III), the peak time varied from 16:00 at 5 cm depth to 1:00 of the next day at 20 cm depth because of heat transport attenuation. Soil temperature had a typical diurnal sinusoidal behavior, and the amplitude decreased with the increase in depth (Bittelli et al., 2008). The soil temperature steadily rose from 26.0°C to 28.8°C with increasing valley values. However, slight rising trends were observed in Experiments I and II with the valley values growth of 1.2°C and 0.7°C, respectively. This result can be explained by the changes in soil thermal conductivity, which is a function of soil water content. Higher moisture content (e.g., in capillary zone) results in higher soil thermal conductivity, which allows easier heat transfer than that in unsaturated zones with lower moisture content. Thus, the accumulated heat in the soil led to a fast temperature increase during the experiment period in Experiment III. This finding is consistent with previous field research conducted by Saito and Šimunek (2009) during the summer. Saito and Šimunek (2009) assumed that the groundwater table is located far below the upper soil layers, especially the root layer, and that heat transfer across the lower boundary occurs only by convection of liquid water and water vapor.

Results indicate that shallow groundwater has a "cooling" effect on soil in the capillary zone, whereas the effect is not evident when groundwater table was more than 60 cm deep. The cooling effect increases with soil moisture content. Given that plant roots and microorganisms are sensitive to soil temperature, the results are significant for the growth of organisms in the soil environment. Thus, control of the soil moisture content could improve the temperature resistance of organisms.

Figure 6 shows soil temperature profiles with diurnal changes. Soil temperature profiles followed the same trend in Experiments I, II, and III. Four types of temperature profiles were observed. The first type was an exothermic profile that occurred at night from 0:00 to 4:00. Given that the soil surface did not receive energy from solar

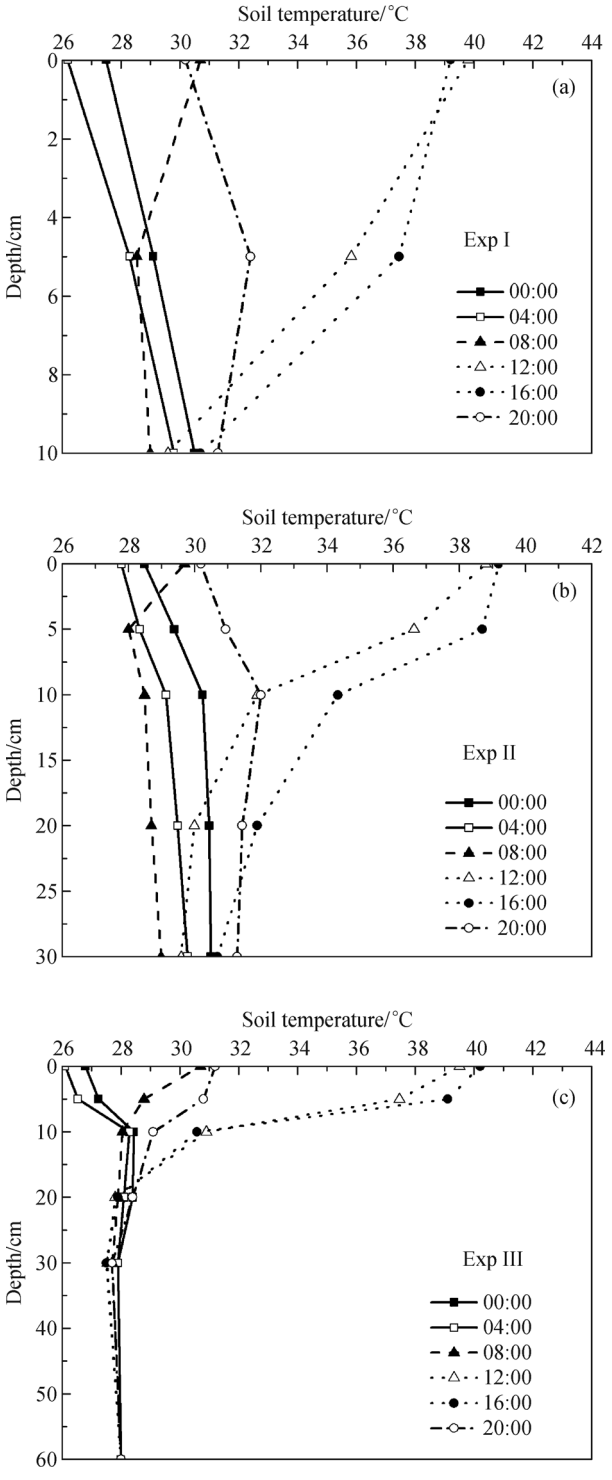

Fig. 6 Different types of soil temperature profiles at day and night above (a) 10 cm, (b) 30 cm, and (c) 60 cm groundwater table depths. Straight lines represent the exothermic type; dotted lines represent the transitional type from exothermic to endothermic; dashed lines depict the endothermic type; and dash-dot lines depict the transitional type from endothermic to exothermic.

shortwave radiation at night, the interior soil temperature was higher than the surface which resulted in a soil temperature decrease at the first time step. The maximum temperature layer was approximately 30°C on the lower boundary (except for Experiment III with 28°C), and the temperature gradient was upward to release heat from the soil interior. The second soil profile was a transitional type from exothermic to endothermic temperature changes, marked by the 8:00 line. The air temperature is higher than the soil temperature, and the soil temperature gradients were upward and downward respectively from the zero gradient layers (Zeng et al., 2009). During this period, the minimum temperature is located at the 5 cm depth. The third temperature profile is an endothermic type, represented by the 12:00 to 16:00 data lines. Zeng (2011) pointed out that heat is absorbed by soil under evaporation conditions and is transferred downward through particles and water vapor in the pores of soil, which results in an increase in temperature in the vertical profile. Given that the endothermic process was not transient but temporal, the temperature near the soil surface increased more evidently than in the lower soil. The fourth temperature profile was a transitional type from the endothermic to the exothermic, marked by the 20:00 data line. The temperature gradients were downward and upward from the maximum temperature layer at 5 cm depth. The dramatic fluctuation of soil profiles were within the top 20 cm depth, especially within the top 10 cm depth.

3.4 Soil thermal properties

Soil thermal parameters depend on the proportion of soil components, size, and range of solid particles. These parameters are related to soil texture, porosity, moisture content, and salinity (de Vries, 1963).

Thermal conductivity is a function of water content and soil temperature based on Eqs. (3) and (4). When the groundwater table was at a 10 cm depth, thermal conductivity was stable at 2.3 $W \cdot cm^{-1} \cdot K^{-1}$ because of the nearly saturated soil with unchanging components. Figure 7 shows that the average values of thermal conductivity calculated for Experiment II were 1.82 $W \cdot cm^{-1} \cdot K^{-1}$, 2.15 $W \cdot cm^{-1} \cdot K^{-1}$, and 2.21 $W \cdot cm^{-1} \cdot K^{-1}$ at 5 cm, 10 cm, and 20 cm depths, respectively, which is higher than those of Experiment III. A possible explanation for this result is that the large water content could increase the hydrate film of soil particles to benefit heat transfer. This result is similar to other simulations based on heat-pulse measurements (Lu and Ren, 2009), which indicate that the new method simulated by the de Vries model and based on soil temperature and moisture content measurements is feasible.

Calculated values of heat capacity as a function of soil moisture content in Eq. (2) are shown in Figs. 8 and 9. The values of heat capacity at the 5 cm depth decreased with the increasing groundwater table depths (Fig. 8). The peak and valley values appeared at 15:00 and 4:00, respectively, and were influenced by the liquid water migration process forced by the temperature gradient. Under the same evaporative demand, the shallower the groundwater table, the stronger the fluctuation of the heat capacity. This leads to the larger amplitude at 5 cm depth in

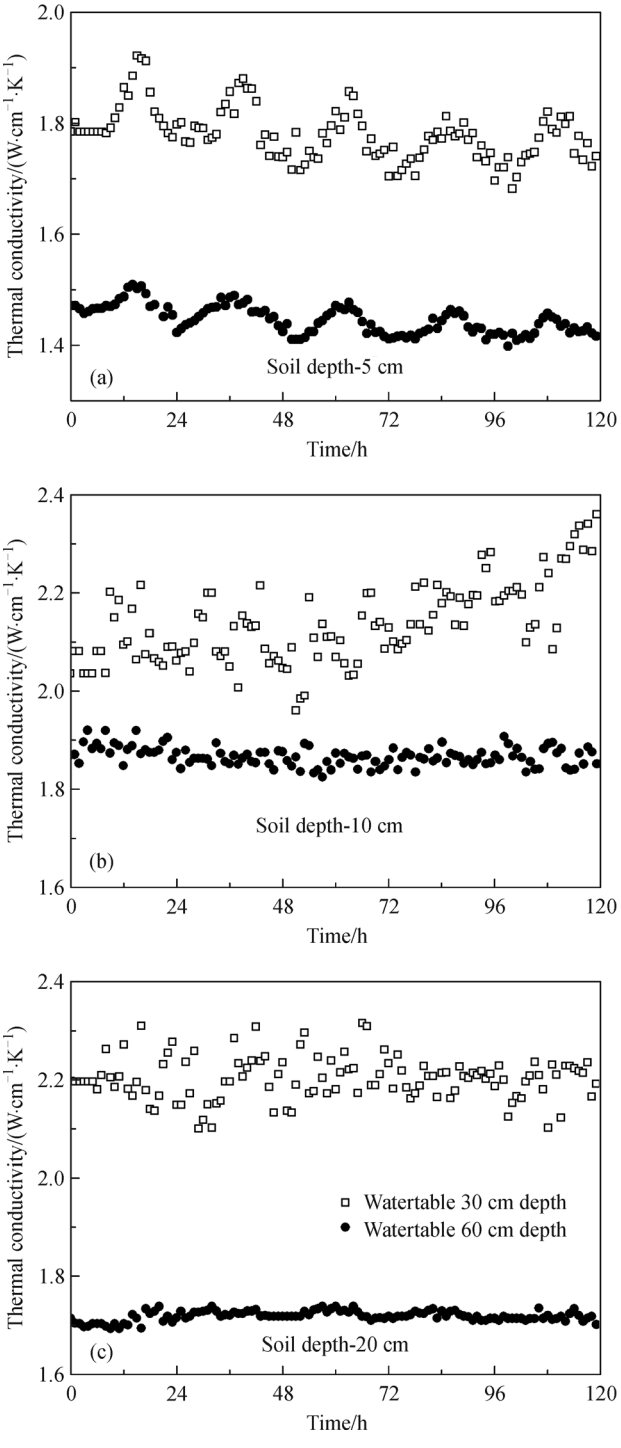

Fig. 7 Changes in thermal conductivity at (a) 5 cm, (b) 10 cm, and (c) 20 cm soil depths above 30 cm and 60 cm groundwater tables.

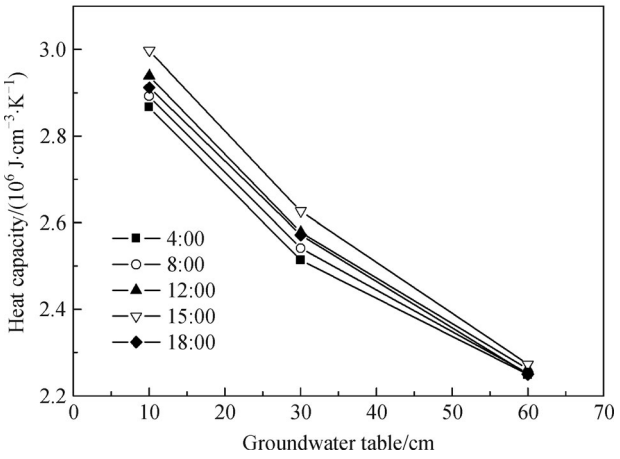

Fig. 8 Heat capacity diurnal changes at shallow vadose zone with increasing groundwater table depth.

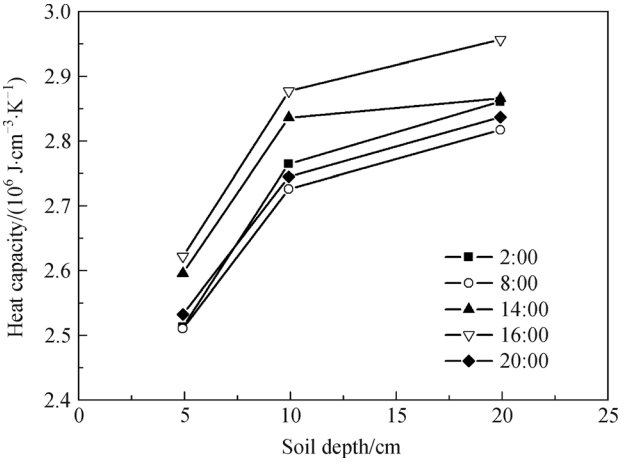

Fig. 9 Heat capacity diurnal changes with increasing soil depth above 30 cm groundwater table (Experiment II).

Experiment I than that in Experiment III with the extent of $0.13\times10^6\,\mathrm{J\cdot cm^{-3}\cdot K^{-1}}$. Figure 9 shows that the heat capacity changed at different observation depths for Experiment II. Heat capacity increased with the increasing depth at each experiment time. At each observation depth, the maximum heat capacity appeared at 16:00, whereas the minimum was at 8:00.

4 Conclusions

Groundwater recharge plays an important role on soil moisture redistribution through capillary water rise during evaporation. Groundwater recharge also greatly affects the soil thermal properties. We measured soil water content and temperature above different shallow groundwater tables and calculated thermal properties based on the de Vries model. Both moisture content and temperature decreased with the increase in groundwater depth and had 24 h diurnal fluctuations for non-isothermal evaporation. The amplitude of the fluctuations decreased with the increasing depth because of the attenuation of heat transport. The lowest values of soil temperature in Experiment III gradually increased from 26.0°C to 28.8°C. However, the trend was not strongly observed in Experiments I and II. In other words, shallow groundwater has a "cooling" effect on the capillary zone of soil profiles. In addition, the thermal conductivity and heat capacity decreased with increasing groundwater table depth, which is consistent with the experiment results. We conducted experiments under controlled conditions to simplify the climatic and hydrographic conditions. The single factor of groundwater influence on soil temperature and water content under non-isothermal evaporation should be studied. Additional complex conditions such as wind speed and precipitation should be considered comprehensively in further research.

Acknowledgements The authors would like to thank National Key Technology R&D Program of the Ministry of Science and Technology, China (No. 2012BAC07B02), for their support and for providing the funds to make this study possible.

References

Barry-Macaulay D, Bouazza A, Singh R M, Wang B, Ranjith P G (2013). Thermal conductivity of soils and rocks from the Melbourne (Australia) region. Eng Geol, 164: 131–138

Bittelli M, Ventura F, Campbell G S, Snyder R L, Gallegati F, Pisa P R (2008). Coupling of heat, water vapor, and liquid water fluxes to compute evaporation in bare soils. J Hydrol (Amst), 362(3–4): 191–205

Bristow K L, Kluitenberg G J, Goding C J, Fitzgerald T S (2001). A small multi-needle probe for measuring soil thermal properties, water content and electrical conductivity. Comput Electron Agric, 31(3): 265–280

Carrera-Hernández J J, Smerdon B D, Mendoza A (2012). Estimating groundwater recharge through unsaturated flow modelling: sensitivity to boundary conditions and vertical discretization. J Hydrol (Amst), 452–453: 90–101

Cass A, Campbell G S, Jones T L (1984). Enhancement of thermal water vapor diffusion in soil. Soil Sci Soc Am J, 48(1): 25–32

Chung S O, Horton R (1987). Soil heat and water flow with a partial surface mulch. Water Resour Res, 23(12): 2175–2186

Daw J E, Rempe J L, Knudson D L (2012). Hot wire needle probe for in-reactor thermal conductivity measurement. IEEE Sens J, 12(8): 2554–2560

De Vries D A (1958). Simultaneous transfer of heat and moisture in porous media. Trans Am Geophys Union, 39(5): 909–916

De Vries D A (1963). The thermal properties of soils. In: van Wijk W R, ed. Physica of Plant Environment. Amsterdam: North-Holland Pub. Co, 210–235

Deb S K, Shukla M K, Sharma P, Mexal J G (2011). Coupled liquid water, water vapor, and heat transport simulations in an unsaturated zone of a sandy loam field. Soil Sci, 176(8): 387–398

Fan Z S, Nefa J C, Harden J W, Zhang T J, Veldhuis H, Czimczik C I, Winston G C, O'Donnell J A (2011). Water and heat transport in boreal soils: implications for soil response to climate change. Science of the Total Environment, 409 (10): 1836–1842

Grifoll J, Gastó J M, Cohen Y (2005). Non-isothermal soil water transport and evaporation. Adv Water Resour, 28(11): 1254–1266

Heilman J L, McInnes K J, Gesch R W, Lascano R J, Savage M J (1996). Effects of trellising on the energy balance of a vineyard. Agr Forest Meteorol, 81(1–2): 79–97

Kane D L, Hinkel K M, Goering D J, Hinzman L, Outcalt S I (2001). Non-conductive heat transfer associated with frozen soils. Global Planet Change, 29(3–4): 275–292

Kang Y, Wang X, Wen J (2014). System for measuring soil thermal conductivity, has soil thermal flux sensor which is arraged between soil temperature sensor and soil moisture sensor that is embedded in soil at specific depth. The patentee: Cold and Arid Regions Environmental and Engineering Research Institute, Patent numbers: CN203337585-U

Kanzari S, Hachicha M, Bouhlila R, Battle-Sales J (2012). Characterization and modeling of water movement and salts transfer in a semi-arid region of Tunisia (Bou Hajla, Kairouan)-Salinization risk of soils and aquifers. Comput Electron Agric, 86: 34–42

Karl T R (1986). The relationship of soil moisture parameterizations to subsequent seasonal and monthly mean temperature in the United States. Mon Weather Rev, 114(4): 675–686

Li C, Qi J, Feng Z, Yin R, Zou S, Zhang F (2010). Parameters optimization based on the combination of localization and auto-calibration of SWAT model in a small watershed in Chinese Loess Plateau. Front Earth Sci, 4(3): 296–310

Lu S, Ren T (2009). Model for predicting soil thermal conductivity at various temperatures. Transactions of the CSAES, 25(7): 13–18 (in Chinese)

Lu S, Ren T, Yu Z, Horton R (2011). A method to estimate the water vapour enhancement factor in soil. Eur J Soil Sci, 62(4): 498–504

Lu Y L, Wang Y J, Ren T S (2013). Using late time data improves the Heat-Pulse method for estimating soil thermal properties with the pulsed infinite line source theory. Vadose Zone J, 12(4): 1–9

Nakhaei M, Šimunek J (2014). Parameter estimation of soil hydraulic and thermal property functions for unsaturated porous media using the HYDRUS-2D code. J hydrol hydromech, 62(1):7–15

Novak M D (2010). Dynamics of the near-surface evaporation zone and corresponding effects on the surface energy balance of a drying bare soil. Agric Meteorol, 150(10): 1358–1365

Philip J R, de Vries D A (1957). Moisture movement in porous materials under temperature gradients. Trans Am Geophys Union, 38(2): 222–232

Rahman A (2008). A GIS based DRASTIC model for assessing groundwater vulnerability in shallow aquifer in Aligarh, India. Appl Geogr, 28(1): 32–53

Rose C W (1968). Water transport in soil with a daily temperature wave. I. Theory and experiment. Aust J Soil Res, 6(1): 31–44

Rose D A, Konukcu F, Gowing J W (2005). Effect of watertable depth on evaporation and salt accumulation from saline groundwater. Aust J Soil Res, 43(5): 565–573

Saito H, Šimunek J (2009). Effects of meteorological models on the solution of the surface energy balance and soil temperature variations in bare soils. J Hydrol (Amst), 373(3–4): 545–561

Saito H, Šimunek J, Mohanty B P (2006). Numerical analysis of coupled water, vapor, and heat transport in the Vadose Zone. Vadose Zone J, 5 (2): 784–800

Shi W, Zeng W, Chen B (2010). Application of visual MODFLOW to assess the sewage plant accident pool leakage impact on groundwater in the Guanting Reservoir area of Beijing. Front Earth Sci, 4(3): 320–325

Šimunek J, Sejna M, van Genuchten M Th (1998). The HYDRUS-1D software packa- ge for simulating the one dimensional movement of water, heat, and multiple solutes in variably-saturated media. Version 2.0. IGWMC-TPS-70. Int. Ground Water Modeling Center, Colorado School of Mines, Golden

Umali D L (1993). Irrigation-Induced Salinity: a Growing Problem for Development and the Environment. Washington, D.C.: World Bank, 22–28

Usowicz B, Lipiec J, Usowicz J B, Marczewski W (2013). Effects of aggregate size on soil thermal conductivity: comparison of measured and model-predicted data. Int J Heat Mass Transfer, 57(2): 536–541

Van Genuchten M Th (1980). A closed-form equation for predicting the hydraulic conductivity of unsaturated soils. Soil Sci Soc Am J, 44(5): 892–898

Waite W F, Gilbert L Y, Winters W J, Mason D H (2006). Estimating thermal diffusivity and specific heat from needle probe thermal conductivity data. Rev Sci Instrum, 77(4): 044904–044904-5

Wang K, Xu X, Gao Q (2010). Hydraulic redistribution in the Inner Mongolia Huangfuchuan basins under different climate scenarios. Front Earth Sci, 4(3): 269–276

Yang C B, Sakai M, Jones S B (2013). Inverse method for simultaneous etermination of soil water flux density and thermal properties with a penta-needle heat pulse probe. Water Resour Res, 49(9): 5851–5864

Zeng Y (2011). Coupled water-vapor-heat transport in the unsaturated soil and its numerical simulation. Beijing: China University of Geosciences, 14–18 (in Chinese)

Zeng Y, Su Z, Wan L, Wen J (2011b). A simulation analysis of the advective effect on evaporation using a two-phase heat and mass flow model. Water Resour Res, 47(10): 529–547

Zeng Y, Wan L, Su Z, Saito H, Huang K, Wang X (2009). Diurnal soil water dynamics in the shallow vadose zone (field site of China University of Geosciences, China). Environ Geol (Environ Geol), 58 (1): 11–23

Zeng Y, SuZ, Wan L, Wen J (2011a). Numerical analysis of air-water-heat flow in unsaturated soil: is it necessary to consider airflow in land surface models? J Geophys Res, 116(D20): 107–125